The Potential Due to a Charged Metallic Strip on a Semiconductor Surface

By E. WASSERSTROM† and J. McKENNA

(Manuscript received December 30, 1969)

We solve numerically the problem of finding the potential and electric field around a negatively charged metallic contact on the surface of an n-type semiconductor. The semiconductor, which has permittivity ϵ_1 *, fills the half-space* $y < 0$*. The contact is an infinitely long strip of width* $2a$*, defined by* $y = 0$, $0 \leqq x \leqq 2a$, $-\infty < z < \infty$*. The region* $y > 0$ *is vacuum with permittivity* ϵ_0 *. In suitable dimensionless coordinates the potential* ϕ *satisfies Laplace's equation in* $y > 0$ *and the equation* $\nabla^2\phi = e^{\phi} - 1$ *in* $y < 0$*. On the boundary* $y = 0$, $\phi = \phi_0 < 0$, $0 \leqq x \leqq 2a$, *and the usual electromagnetic boundary conditions at the remainder of the interface. Finite difference schemes are used to solve the resulting boundary value problem.*

In most practical cases $|\phi_0| \gg 1$ *and* $\eta = \epsilon_0/\epsilon_1 \ll 1$*. We examine in considerable detail the limiting case* $\eta = 0$*, first for the less practical situation where* $|\phi_0| \ll 1$ *and then for* $|\phi_0| \gg 1$*. In case the* $|\phi_0| \ll 1$ *we show that our numerical solution agrees well with the exact analytical solution of a linearized version of the problem. For* $|\phi_0| \gg 1$*, we give plots of the equipotential curves, curves of equal charge density, and curves of constant electric field amplitude. These results also yield expressions for the capacitance of both a strip and a circular electrode. The modifications of these results when* $\eta > 0$ *are also given in some detail. Finally, we discuss the numerical calculations at some length.*

I. INTRODUCTION AND FORMULATION OF THE PROBLEM

In the study of a number of solid-state devices, it is important to know the electrostatic potential in the neighborhood of a metal-semiconductor contact (Schottky diode) and in a metal insulator-semiconductor structure (MOS capacitor).

Motivated by this interest, we consider in this paper the following

† On leave from the Technion-Isreal Institute of Technology, Haifa, Israel, when this work was conducted.

problem. An infinitely long metallic strip of width $2a^*$ and zero thickness occupies the region $0 \leqq x^* \leqq 2a^*$, $y^* = 0$, as shown in Fig. 1. The region $y^* > 0$ is filled with air and the region $y^* < 0$ is filled with an n-type semiconductor. The metallic strip is charged to a negative potential, $\phi_0^* < 0$, and we wish to calculate the potential, the electric field and the electric charge density distribution in the semiconductor under the assumption of no current flow. As will be shown later, this solution also determines the potential, field and charge density around a circular metallic contact.

For the doping levels normally encountered in such devices, say 10^{20}–10^{22} m^{-3} the electrostatic potential ϕ^* in the semiconductor is governed by the Poisson equation,

$$\nabla^{*2}\phi^* = -\rho^*/\epsilon_1 , \tag{1}$$

where ∇^{*2} is the Laplacian, ϵ_1 is the permittivity of the semiconductor, and the net volume charge density ρ^* is given by[1]

$$\rho^* = qN_d[1 - \exp(q\phi^*/kT)], \tag{2}$$

where $-q$ is the charge of an electron, N_d is the donor number density, k is Boltzmann's constant, and T is the absolute temperature. In writing down equation (2) we have neglected the contact potential Ψ between the metal strip and the semiconductor,[2] since in many cases of practical interest $|\phi_0| \gg |\Psi|$. Here and in the following, starred quantities have rationalized MKS dimensions; unstarred quantities, except for a few obvious physical parameters, are dimensionless.

As in Ref. (1) we introduce the dimensionless length and potential

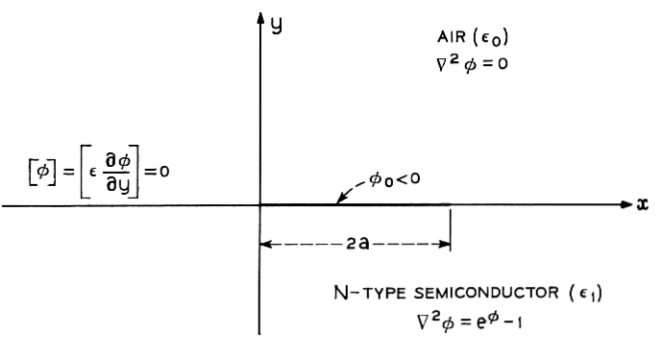

Fig. 1—A diagram of the geometry of the problem Pl showing the conducting strip at the air-semiconductor interface and the coordinate system used. The dimensionless parameters shown are defined in equation (3). The symbol [ ] is defined in equation (8).

by the relations

$$x = x^*/\lambda_D , \qquad y = y^*/\lambda_D , \qquad a = a^*/\lambda_D , \tag{3}$$
$$\phi = q\phi^*/kT, \qquad \rho = \rho^*/qN_d ,$$

where the Debye length is given by[3]

$$\lambda_D = (\epsilon_1 kT/q^2 N_d)^{\frac{1}{2}}. \tag{4}$$

Typical values for a lightly doped semiconductor device are $N_d = 10^{21}\ m^{-3}$, $\epsilon_0/\epsilon_1 = .0625$ for germanium and $\epsilon_0/\epsilon_1 = .078$ for silicon, and $a^* = 10^{-4}\ m$, where ϵ_0 is the permittivity of free space. Then, for example, for silicon at $T = 300°\text{K}$, $\lambda_D = 1.35 \times 10^{-7}$ m, $q/kT = 38.8$ volt^{-1}, and $a = 740$.

In terms of these dimensionless quantities the boundary value problem to be solved for the potential ϕ can be summarized mathematically as follows:

(*i*) In the air, $y > 0$ (see Fig. 1), the potential satisfies Laplace's equation

$$\nabla^2\phi = 0. \tag{5}$$

(*ii*) In the semiconductor, $y < 0$, the potential satisfies Poisson–Boltzman's equation

$$\nabla^2\phi = e^{\phi} - 1. \tag{6}$$

(*iii*) On the plate, $y = 0$ and $0 \leqq x \leqq 2a$, the potential is a given (negative) constant

$$\phi = \phi_0 < 0. \tag{7}$$

(*iv*) At the interface, $y = 0$, $|x - a| > a$, the potential and the normal component of the electric displacement vector are continuous[4]

$$[\phi(x, 0)] = \phi(x, 0+) - \phi(x, 0-) = 0, \tag{8a}$$

$$\left[\epsilon \frac{\partial\phi}{\partial y}(x, 0)\right] = \eta \frac{\partial\phi}{\partial y}(x, 0+) - \frac{\partial\phi}{\partial y}(x, 0-) = 0, \tag{8b}$$

where

$$\eta = \epsilon_0/\epsilon_1 . \tag{8c}$$

(*v*) At infinity

$$\lim_{r\to\infty} (\phi) = 0, \tag{9}$$

where $r = (x^2 + y^2)^{\frac{1}{2}}$.

We refer to the boundary value problem defined by conditions (*i*)–(*v*) as P1. We have been unable to solve this problem analytically, and instead have studied its solution numerically.

Qualitatively, for large $|\phi_0|$ the potential can be described easily. Within the semiconductor, the negative charge on the conducting strip repels the mobile electrons. This action produces a layer around the strip, called the depletion layer, from which almost all the mobile electrons have been expelled. The positive donor ions left behind make this a region of uniform positive volume charge density. Far from the plate the semiconductor is almost neutral, and these two regions are connected by a transition layer. When $\eta = 0$ this transition layer is sharp and well defined and is several Debye lengths thick. However, when $\eta \neq 0$, this transition region becomes broader and diffuse near the semiconductor-air interface. In the air on the other hand, the potential is essentially that due to the dipole formed by the negative charge on the conducting strip and the positive charge due to the donor ions in the depletion layer.

In Section II, we consider the special case $\eta = 0$. For bias voltages ϕ_0 which are typically encountered in semiconductor devices, the thickness of the depletion layer is large compared to a Debye length but small compared to the width of the strip, $2a$. We will show that we then only need to consider a strip completely embedded in an n-type semiconductor. This will reduce the solution of P1 to the solution of P2

(*i*) In the semiconductor $\nabla^2\phi = e^{\phi} - 1.$ (6)

(*ii*) On the plate, $y = 0, 0 \leqq x \leqq 2a, \phi = \phi_0 < 0.$ (10)

(*iii*) At infinity $\lim_{r\to\infty} (\phi) = 0.$ (11)

Solutions of P2 are obtained by the method of finite differences. For $|\phi_0| \ll 1$, equation (6) can be linearized to

$$\nabla^2\phi = \phi. \tag{12}$$

The linearized version of P2 in the limit $a = \infty$, has been solved analytically by Lewis[5] and for small ϕ_0 his results agree excellently with our numerical solution in the region $x < a$. This provides a good check on our numerical methods. Note, however, that in our formulation we neglected the contact potential and therefore the problem is not physically meaningful for this limit. For $|\phi_0| \gg 1$ numerical calculations of both the electric field and the potential are presented in considerable detail. Finally, the capacitance per unit length of the strip and the capacitance of a circular electrode are presented with particular emphasis on edge effects.

In Section III we briefly discuss what modifications of the results of Section II must be made when $\eta \neq 0$. It is shown that the chief effect of positive η in the semiconductor is a smearing out of the transition region near the air-semiconductor interface.

In Section IV we give some of the details of the methods of numerical analysis used.

II. THE CASE $\eta = 0$

In most practical applications $\epsilon_0 \ll \epsilon_1$, as was pointed out in Section I, and it is therefore of interest to treat first the simpler, limiting problem with $\eta = 0$. When $\eta = 0$ condition (8b) becomes

$$\frac{\partial \phi}{\partial y}(x, 0-) = 0, \tag{13}$$

and the solution for the potential in the semiconductor is decoupled from the solution for the potential in the air. In fact, the solution of P1 in the semiconductor is now identical with the solution of P2 because of symmetry.

There are three characteristic lengths in the problem of the finite width strip: the half width of the strip, the Debye length, and the thickness of the depletion layer. If the half width of the strip is very large compared to both the Debye length and the thickness of the depletion layer, the solution below the plate and sufficiently far from the edges must be the one dimensional solution (independent of x). Thus, for a "sufficiently wide" finite strip, there are really only two characteristic lengths for the solution in the semiconductor: the Debye length and the depletion layer thickness.

We determine more precisely what "sufficiently wide" means. It is well known that if one considers the one dimensional problem of an n-type semiconductor filling the region $y < 0$, with the plane $y = 0$ held at a large negative potential $\phi_0 < 0$, then the thickness of the depletion layer, R, is accurately given by[2]

$$R = |2\phi_0|^{\frac{1}{2}}. \tag{14}$$

[The accuracy of this approximation is also discussed in Ref. (1).] The Debye length is equal to unity in our nondimensional coordinates. Thus, if in addition to $\eta = 0$, we have

$$a \gg 1, \tag{15a}$$

and

$$a \gg R, \tag{15b}$$

then a disappears from the problem in the semiconductor as a characteristic length. Reverse bias voltages of the order of $\phi_0^* \sim -5$ to -50 volts, ($\phi_0 \sim -200$ to -2000) are typical, and this corresponds to $R \sim 19.7$ to 63.0 at room temperature. Thus in most practical situations condition (15) is satisfied, since $a \gtrsim 740$, and we can expect the solutions to be independent of a also near the edges of the strip.

If in addition to equations (13) and (15a) we have

$$|\phi_0| \ll 1, \tag{16}$$

then P2 can be linearized, for equation (5) can be approximated by

$$\nabla^2\phi = \phi, \tag{17}$$

since $|\phi| \leqq |\phi_0|$ everywhere. This linear problem with $a = \infty$ has been solved analytically by Lewis,[5] and in polar coordinates (see Fig. 2) the solution is given by

$$\phi/\phi_0 = \tfrac{1}{2}\exp(r\sin\theta)\left\{1 - \operatorname{erf}\left[r^{\frac{1}{2}}\left(\cos\frac{\theta}{2} + \sin\frac{\theta}{2}\right)\right]\right\} + \tfrac{1}{2}\exp(-r\sin\theta)\left\{1 + \operatorname{erf}\left[r^{\frac{1}{2}}\left(\cos\frac{\theta}{2} - \sin\frac{\theta}{2}\right)\right]\right\}, \tag{18}$$

where erf (z) is the error function.[6] We have solved the (nonlinear) P2 by a finite difference method to be described in Section IV. The numerically calculated equipotentials are shown in Fig. 3, and in Fig. 4 we compare the numerical solution of P2 (crosses) with the analytical solution (18) of the linearized problem (continuous line).

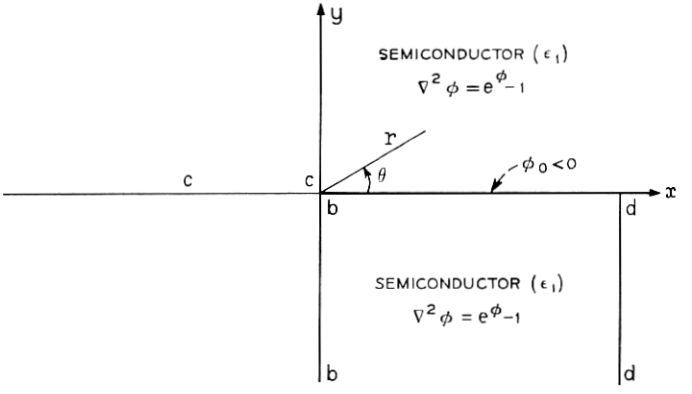

Fig. 2—A diagram of the geometry of the problem P2 showing the coordinate system used.

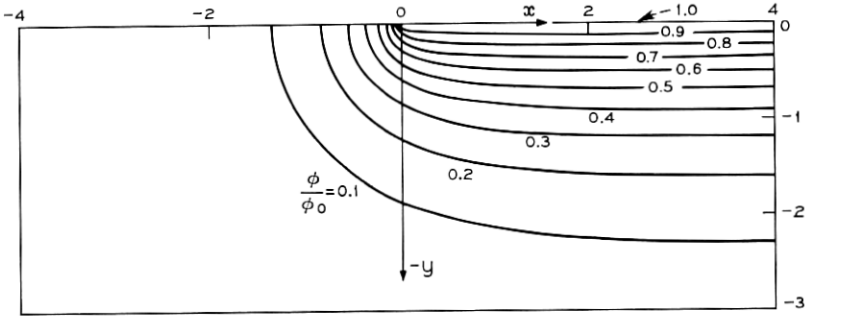

Fig. 3—Equipotential curves for the case $\eta = 0$, $\phi_0 = -.01$, and $a = 4$.

These figures correspond to $\phi_0 = -.01$ and $a = 4$, using the mesh size $\Delta x = \Delta y = .1$. The three curves in Fig. 4 are the potential along the lines $b - b(x \leqq 0, y = 0)$, $c - c(x = 0, y \leqq 0)$ and $d - d(x = 4, y \leqq 0)$. These three lines are shown in Fig. 2. It is seen that the two solutions agree very well.

In most practical cases, however, ϕ_0 is very large (typically $200 < |\phi_0| < 2000$), so we shall concentrate on the large potential problem from now on. When ϕ_0 is not small, the problem cannot be linearized. We have been unable to find approximate analytic solutions, and so we have had to solve the problem numerically.

From the results of Ref. (1), we should expect that if distances are normalized with respect to the depletion layer thickness, then the potential when normalized with respect to the plate potential should be essentially independent of ϕ_0 as $|\phi_0| \to \infty$. We introduce this normalization here:

$$\tilde{x} = x/R, \qquad \tilde{y} = y/R, \qquad \tilde{a} = a/R, \qquad \tilde{\phi} = \phi/\phi_0\,, \qquad \tilde{\rho} = \rho, \tag{19}$$

where R is the depletion layer thickness given in equation (14). In terms of our new variables, the basic equation (6) for $\tilde{\phi}(\tilde{x}, \tilde{y})$ reads

$$\tilde{\nabla}^2\tilde{\phi} \equiv \left(\frac{\partial^2}{\partial\tilde{x}^2} + \frac{\partial^2}{\partial\tilde{y}^2}\right)\tilde{\phi} = 2(1 - e^{\phi_0\tilde{\phi}}) = 2\tilde{\rho}. \tag{20}$$

We have solved P2 in the normalized (tilde) variables by the method of finite differences. A detailed description of the method will be given in Section IV. Calculations for $\phi_0 = -100$ and -500 using the mesh sizes $\Delta\tilde{x} = \Delta\tilde{y} = .05$ and for $\phi_0 = -2500$ using the mesh sizes $\Delta\tilde{x} = \Delta\tilde{y} = .025$ for $\tilde{a} = 3$ and 4, have been carried out. In Fig. 5 we show the equipotential ($\tilde{\phi}$) lines and in Fig. 6 the lines of constant charge $\tilde{\rho}(=\rho)$

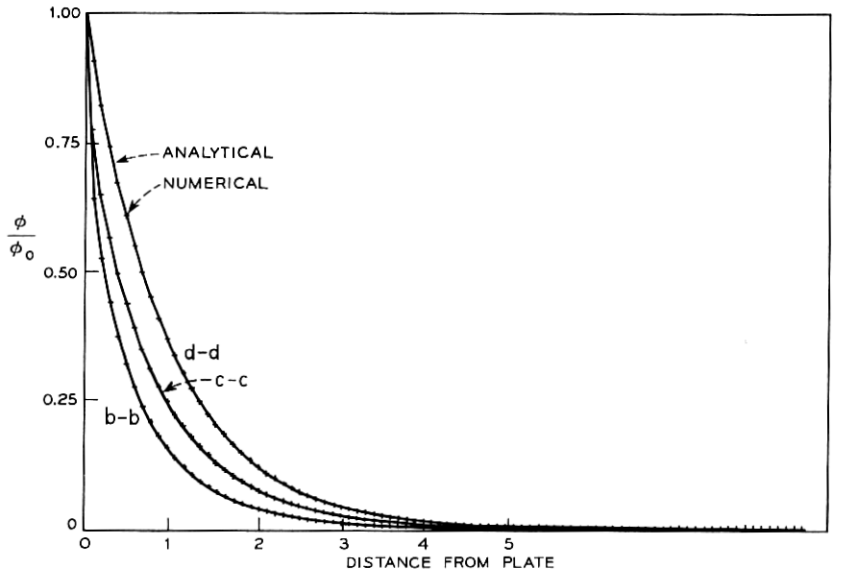

Fig. 4—A comparison of the analytical solution of the linearized problem (continuous line) with the numerical solution of the nonlinear problem P2 (crosses) for the case $\eta = 0$, $\phi_0 = -.01$. The three curves are the potential along $b - b$ ($x \leqq 0$, $y = 0$), $c - c$ ($x = 0$, $y \leqq 0$) and $d - d$ ($x = 4$, $y \leqq 0$).

for the case $\phi_0 = -500$. These curves show clearly the depletion layer and the transition layer. The curves for $\phi_0 = -100$ and -2500 (which we do not show) are essentially the same; they differ only in that for $\phi_0 = -100$ the transition layer is thicker while for $\phi_0 = -2500$ it is sharper. It might be pointed out that in the tilde coordinates the thickness of the transition layer becomes vanishingly small as $|\phi_0| \to \infty$,

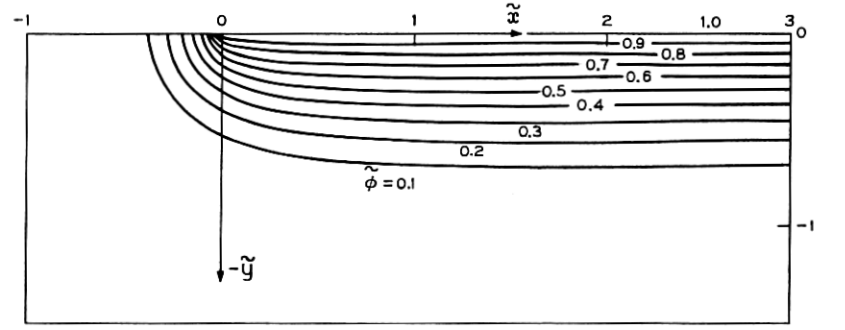

Fig. 5—Equipotential curves for the case $\eta = 0$, $\phi_0 = -500$, $\bar{a} = 3$.

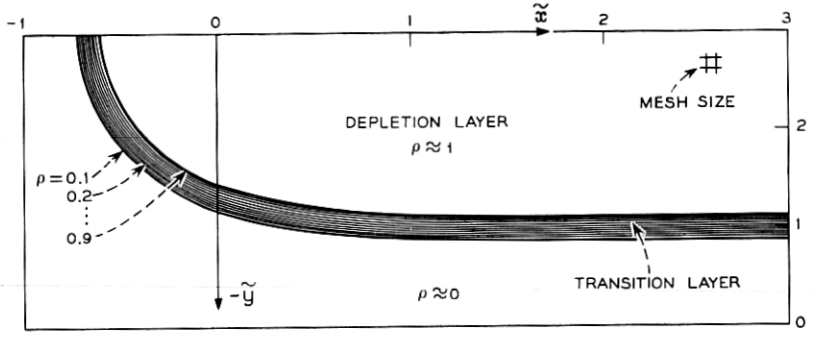

Fig. 6—Constant charge density curves for the case $\eta = 0, \phi_0 = -500$ and $\tilde{a} = 3$.

but in the true dimensional coordinates, the thickness is $\sim 4\lambda_D$, independent of ϕ_0 as $|\phi_0| \to \infty$.

Figures 5 and 6 also show that for $\tilde{x} \gtrsim 2$, the equipotential and equicharge curves are essentially parallel to the $\tilde{x}$ axis. Thus $a \gtrsim 2R$ is a sufficient condition for replacing the strip of finite width by a semi-infinite strip. Furthermore, since $\partial\tilde{\phi}/\partial\tilde{x} = \partial^2\tilde{\phi}/\partial\tilde{x}^2 = 0$ in the region $\tilde{x} \gtrsim 2$, the solution is one dimensional here. In Ref. (1) it was shown that an excellent approximate solution of the one dimensional problem is the "zeroth-order matching" solution

$$\tilde{\phi} = \begin{cases} (1 - |\tilde{y}|)^2, & -1 \leqq \tilde{y} \leqq 0 \\ 0, & \tilde{y} \leqq -1. \end{cases} \tag{21}$$

From equation (21) we also see that for $\tilde{x} \geqq 2$

$$\begin{aligned} \tilde{E}_{\tilde{x}} &= -\frac{\partial\tilde{\phi}}{\partial\tilde{x}} = 0, \\ \tilde{E}_{\tilde{y}} &= -\frac{\partial\tilde{\phi}}{\partial\tilde{y}} = \begin{cases} -2(1 - |\tilde{y}|), & -1 \leqq \tilde{y} \leqq 0, \\ 0, & \tilde{y} \leqq -1. \end{cases} \end{aligned} \tag{22}$$

In Fig. 7 we plot $\tilde{\phi}$ along the lines $b - b(\tilde{x} \leqq 0, \tilde{y} = 0)$ $c - c(\tilde{x} = 0, \tilde{y} \leqq 0)$ and $d - d(\tilde{x} = 3, \tilde{y} \leqq 0)$ for the case $\phi_0 = -500$ and $\tilde{a} = 3$. We superimpose on this a plot of $\tilde{\phi}(3, \tilde{y})$ as given by (21). The agreement on $d - d$ between $\tilde{\phi}$ calculated by the finite difference method and $\tilde{\phi}$ given by (21) is excellent. This will be the case even for larger mesh sizes since the truncation error due to approximating the Laplacian by a five point difference scheme is proportional to the fourth derivatives of $\tilde{\phi}$, which should be small since $\tilde{\phi}$ is essentially parabolic along $d - d$.

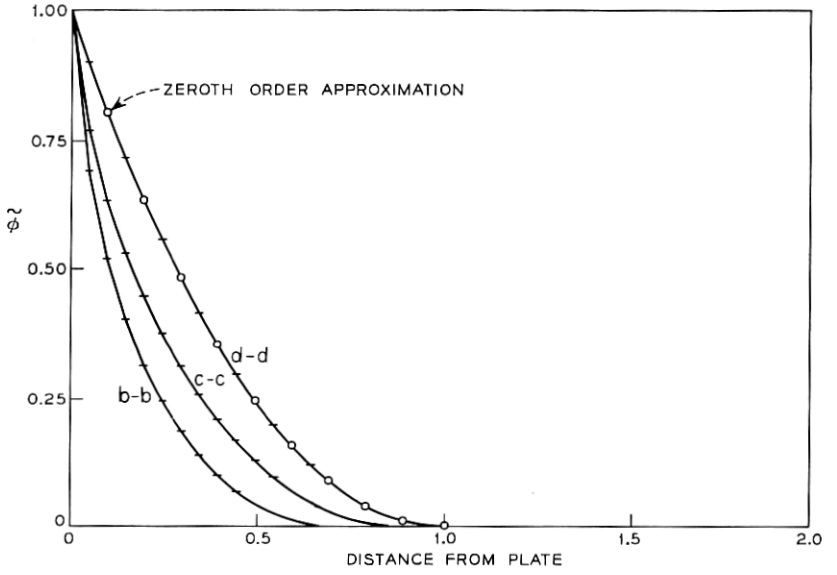

Fig. 7—Graphs of $\tilde{\phi}$ along the lines $b - b$ ($\tilde{x} \leqq 0$, $\tilde{y} = 0$), $c - c$ ($\tilde{x} = 0$, $\tilde{y} \leqq 0$) and $d - d$ ($\tilde{x} = 3$, $\tilde{y} \leqq 0$) for the case $\eta = 0$, $\phi_0 = -500$, and $\tilde{a} = 3$. Superimposed on the $d - d$ curve is a plot of $\tilde{\phi}(3, \tilde{y})$ (circles) given by equation (21).

In Fig. 8 we plot $|\tilde{E}_{\tilde{x}}|$ along $b - b$ and $|\tilde{E}_{\tilde{y}}|$ along $c - c$ and $d - d$ for the same case, and we superimpose on this a plot of $|\tilde{E}_{\tilde{y}}(3, \tilde{y})|$ as given by equation (22).

Because of the singularities of the electric field (and all higher derivatives of the potential) near the edge $\tilde{x} = \tilde{y} = 0$, one cannot expect to obtain a uniformly valid numerical solution there. Nevertheless, comparison of the numerical and analytical solutions for the small potential case (Fig. 4) shows that even at the nearest mesh points to the plate edge, the error in the numerical computation of the potential is not large. The error in calculating the electric field is naturally greater. In order to decrease the truncation error (the difference between the exact solution of the differential equation and the solution of the difference equations), one can decrease the mesh size uniformly over the computational field. This can become quite expensive and is not necessary. A more efficient scheme is to refine the mesh size only in a small region around the plate edge and to find the numerical solution inside this region using at the boundary the values obtained from the coarser grid. We have done this for a region of size 1×1 around the plate edge with a mesh size of $\Delta\tilde{x} = \Delta\tilde{y} = .0125$ in the case $\phi_0 = -500$ and $\tilde{a} = 3$.

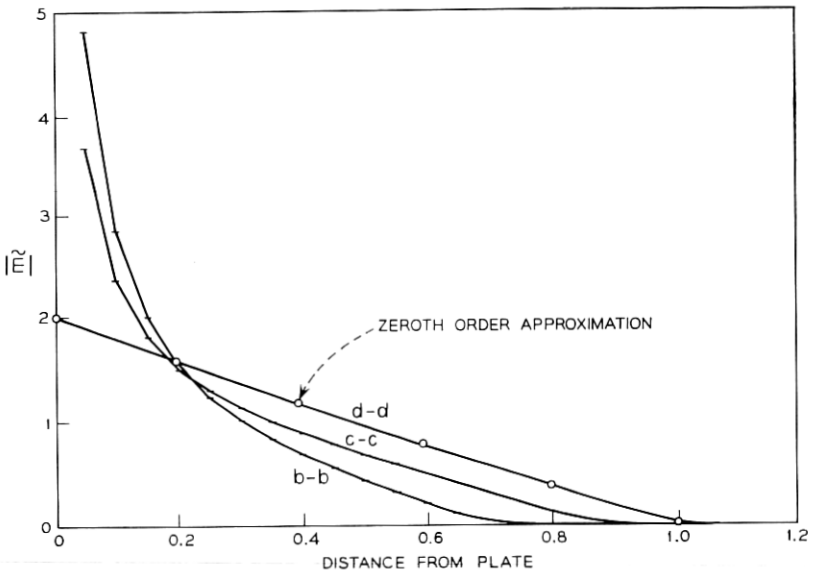

Fig. 8—A plot of $|\tilde{E}_{\tilde{x}}|$ along $b - b(\tilde{x} \leqq 0, \tilde{y} = 0)$ and $|\tilde{E}_{\tilde{y}}|$ along $c - c(\tilde{x} = 0. \tilde{y} \leqq 0)$ and $d - d$ $(\tilde{x} = 3, \tilde{y} \leqq 0)$ for the case $\eta = 0$, $\phi_0 = -500$, and $\tilde{a} = 3$. Superimposed on the $d - d$ curve is a plot (circles) of $|\tilde{E}_{\tilde{y}}(3, \tilde{y})|$ given by equation (22).

For this refined solution we plot $\tilde{\phi}$ along $b - b$ and $c - c$ in Fig. 9, and in Fig. 10 we plot $|\tilde{E}_{\tilde{x}}|$ along $b - b$ and $|\tilde{E}_{\tilde{y}}|$ along $c - c$. The squares are points obtained from the solution using the coarser mesh ($\Delta\tilde{x} = \Delta\tilde{y} = .05$), and we see that several grid points away from the plates, the two solutions agree nicely.

In addition to equipotential curves, curves of constant field amplitude can also be plotted. We define

$$\tilde{\psi}(\tilde{x}, \tilde{y}) = \left[\left(\frac{\partial\tilde{\phi}}{\partial\tilde{x}}\right)^2 + \left(\frac{\partial\tilde{\phi}}{\partial\tilde{y}}\right)^2\right]^{\frac{1}{2}} = ||\,\tilde{\mathbf{E}}\,||. \tag{23}$$

From equation (23) we see that $\max_{\tilde{y}} \tilde{\psi}(\tilde{x}, \tilde{y}) = \tilde{\psi}(\tilde{x}, 0) = 2$ for $\tilde{x} \gtrsim 2$. Near the plate edge, however, there are much higher fields. In Fig. 11 we draw the curves of constant $\tilde{\psi}$, again for the case $\phi_0 = -500$ and $\tilde{a} = 3$. The plate edge region can be defined as the region where $\tilde{\psi}(\tilde{x}, \tilde{y}) \geqq 2$. In Fig. 12 we show in more detail the curves of constant $\tilde{\psi}$ in the plate edge region. The data is taken from the calculation of the potential using a refined mesh around the plate edge discussed above.

An important application of the numerical solution is the computation

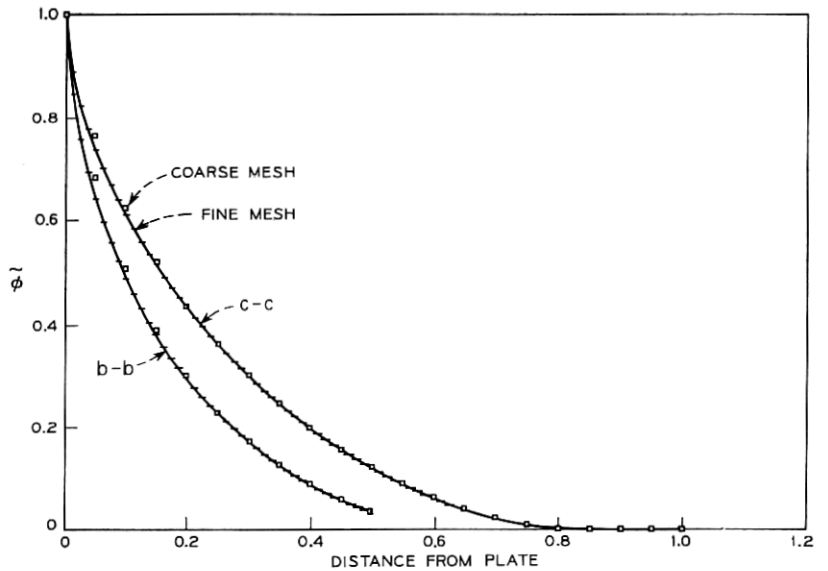

Fig. 9—Plots of $\tilde{\phi}$ along $b - b$ ($\tilde{x} \leqq 0$, $\tilde{y} = 0$) and $c - c$ ($\tilde{x} = 0$, $\tilde{y} \leqq 0$) for the case $\eta = 0$, $\phi_0 = -500$, and $\bar{a} = 3$. The solutions were obtained with a mesh size of $\Delta\tilde{x} = \Delta\tilde{y} = .0125$ (continuous line) and $\Delta\tilde{x} = \Delta\tilde{y} = .05$ (squares).

of the capacitance per unit length of the strip, C^*, where

$$C^* = \frac{\partial Q^*}{\partial \phi_0^*}, \tag{24}$$

and Q^* is the total (dimensional) charge per unit length on the strip. To calculate Q^* we note that it is just equal and opposite to the total net charge per unit length in the semiconductor:

$$Q^* = -\int_{-\infty}^{0} \int_{-\infty}^{\infty} \rho^*(x^*, y^*)\, dx^*\, dy^*. \tag{25}$$

We introduce the nondimensional (tilde) coordinates normalized to the depletion layer thickness and write

$$Q^* = -qN_a\lambda_D^2 R^2 \int_{-\infty}^{0} \int_{-\infty}^{\infty} \tilde{\rho}\, d\tilde{x}\, d\tilde{y} = 2\epsilon_1\phi_0^* \int_{-\infty}^{0} \int_{-\infty}^{\infty} \tilde{\rho}\, d\tilde{x}\, d\tilde{y}. \tag{26}$$

This last integral, which is almost independent of ϕ_0^* for large $|\phi_0^*|$, was computed numerically by evaluating the sum $\sum \sum \tilde{\rho}\ \Delta\tilde{x}\ \Delta\tilde{y}$ and we write the result in the form

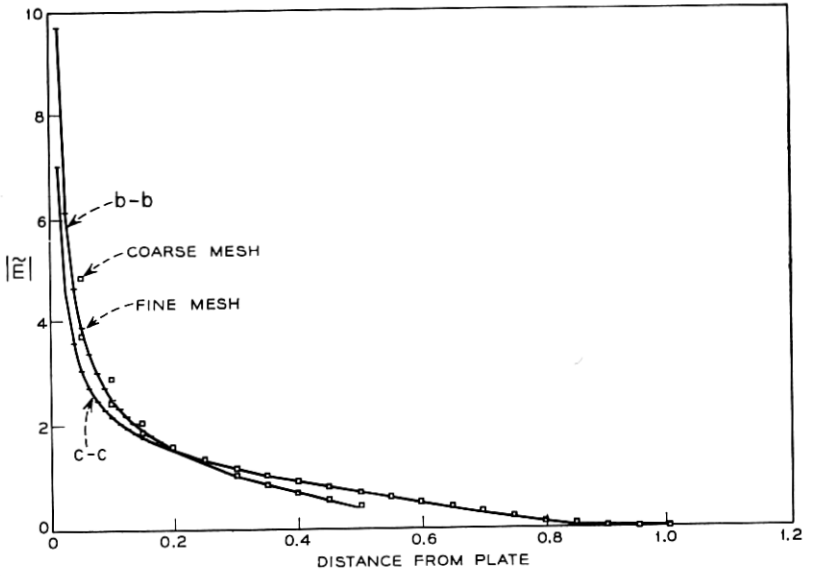

Fig. 10—Plots of $|\tilde{E}_{\tilde{x}}|$ along $b - b(\tilde{x} < 0, \tilde{y} = 0)$ and $|\tilde{E}_{\tilde{y}}|$ along $c - c(\tilde{x} = 0, \tilde{y} \leqq 0)$ for the case $\eta = 0, \phi_0 = -500$, and $\tilde{a} = 3$. The solutions were obtained with a mesh size of $\Delta\tilde{x} = \Delta\tilde{y} = .0125$ (continuous line) and $\Delta\tilde{x} = \Delta\tilde{y} = .05$ (squares).

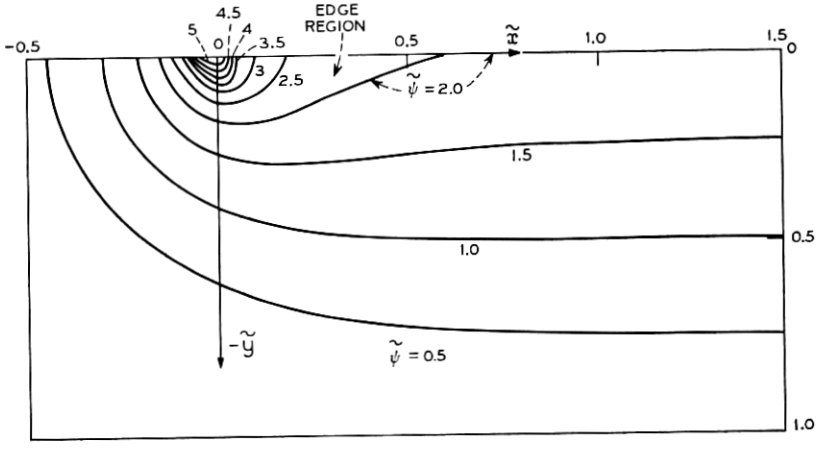

Fig. 11—Curves of constant field amplitude for the case $\eta = 0, \phi_0 = -500$, and $\tilde{a} = 3$.

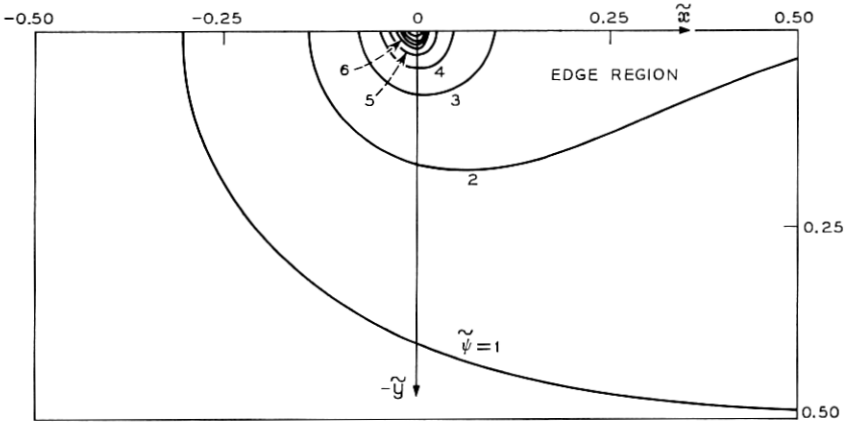

Fig. 12—A detailed plot of the constant field curves near the edge of the plate for the case $\eta = 0$, $\phi_0 = -500$ and $\tilde{a} = 3$.

$$\iint \tilde{\rho}\, d\tilde{x}\, d\tilde{y} = 2\tilde{a} + 2D_0 . \tag{27}$$

The first term on the right of equation (27) is the value we would obtain if the effects of the edges and the transition layer were ignored, and D_0 is the correction for these effects. For $\tilde{a} \gg 1$ and $|\phi_0| \gg 1$, D_0 should be essentially independent of $\tilde{a}$ and ϕ_0, that is, of a^* and ϕ_0^*. For our basic computation, $\tilde{a} = 3$, $\phi_0 = -500$ and $\Delta\tilde{x} = \Delta\tilde{y} = .05$, we obtained

$$D_0 = 0.354. \tag{28}$$

This value of D_0 was very insensitive to increasing $\tilde{a}$ to 4, and it changed only slightly when $|\phi_0|$ was increased to 2500 (with $\Delta\tilde{x} = \Delta\tilde{y} = .025$). When we insert equation (27) into (26), expressing $\tilde{a}$ in dimensional coordinates, we obtain

$$Q^* = 4\epsilon_1\phi_0^*\left(\frac{a^*}{R^*} + D_0\right), \tag{29}$$

where

$$R^* = \lambda_D R = (-2\epsilon_1\phi_0^*/qN_d)^{\frac{1}{2}} \tag{30}$$

is the dimensional depletion layer thickness. From equations (24), (29) and (30) we get

$$C^* = \frac{2a^*\epsilon_1}{R^*}\left(1 + 2D_0\frac{R^*}{a^*}\right). \tag{31}$$

It is clear that our calculations also give an accurate approximation to the potential around a conducting disc of radius r_0^*, situated at the air-semiconductor interface, and charged to a large negative potential, as long as

$$r_0 \gg R, \tag{32}$$

where

$$r_0 = r_0^*/\lambda_D . \tag{33}$$

In all previous expressions for the potential and fields we need only interpret x^* as the radial coordinate r^*.

We can now also calculate the capacitance of a circular disc. In this case we have

$$Q^* = -qN_d\lambda_D^3 R^3 \int_{-\infty}^{0}\int_{-\infty}^{\infty}\int_{-\infty}^{\infty} \tilde{\rho}\, d\tilde{x}\, d\tilde{y}\, d\tilde{z}, \tag{34}$$

and

$$\int_{-\infty}^{0}\int_{-\infty}^{\infty}\int_{-\infty}^{\infty} \tilde{\rho}\, d\tilde{x}\, d\tilde{y}\, d\tilde{z} = \pi\tilde{r}_0^2 + 2\pi\tilde{r}_0 D_0 , \tag{35}$$

where

$$\tilde{r}_0 = r_0/R, \tag{36}$$

and of course we still have $D_0 = 0.354$. If we substitute equations (35) and (36) into (34) and differentiate with respect to ϕ_0^*, we get

$$C^* = \frac{\epsilon_1 \pi r_0^{*2}}{R^*}\left(1 + 4D_0\frac{R^*}{r_0^*}\right). \tag{37}$$

Finally, the potential in the air, $\tilde{y} > 0$ is related to the potential on the interface $\tilde{\phi}(\tilde{x}, 0)$ by Green's formula[7]

$$\tilde{\phi}(\tilde{x}, \tilde{y}) = \frac{1}{\pi}\int_{-\infty}^{\infty} \tilde{y}[(\tilde{x} - \xi)^2 + \tilde{y}^2]^{-1}\tilde{\phi}(\xi, 0)\, d\xi, \tag{38}$$

where implicit use has been made of boundary condition (8a). Using the values of $\tilde{\phi}(\xi, 0)$ obtained from the finite difference solutions in $\tilde{y} < 0$, the integral in (38) has been evaluated numerically to give the potential in $\tilde{y} > 0$.

III. THE CASE $\eta \neq 0$

When $\eta = \epsilon_0/\epsilon_1$ is not zero, the problem of solving P1 is complicated by the fact that the solutions for the potential in the air and in the

semiconductor become coupled and cannot be found separately. Nevertheless, the effects of this coupling can be taken into account in the semiconductor, without actually solving the problem in the air, by using Green's formula (38). We did this and found the solution in the semiconductor by an iterative finite difference scheme. Using this solution on the boundary, the integral in (38) was evaluated numerically to obtain the solution in the air. The details of this numerical scheme are given in Section IV. We continue to concentrate on the case of large potential ($|\phi_0| \gg 1$) and a wide conductiong strip ($a \gg R$), so the normalized (tilde) variables introduced in equation (19) are retained.

Except in a wedge shaped region at the interface at each edge of the strip (see Fig. 13), the solution in the semiconductor is very insensitive to changes in η and is little different from the solution for $\eta = 0$. The main new feature of the solution in the semiconductor is the appearance of a "shoulder" in the depletion layer near the surface, and a smearing out of the transition layer there. In fact, the larger η is, the less sharp the transition layer in this region is. This effect increases the charge in the wedges and thus also increases the capacitance of the plate. The solution in the air is, however, more sensitive to changes in η.

We illustrate these qualitative remarks by a number of graphs. The case illustrated in all these graphs is $\phi_0 = -500$, $\tilde{a} = 3$, and the mesh size used was $\Delta\tilde{x} = \Delta\tilde{y} = .05$. In Fig. 14 we show the equipotential ($\tilde{\phi}$) curves and in Fig. 13 we show the curves of constant charge ($\tilde{\rho}$) for $\eta = .1$. These two figures illustrate the previous remarks. In Fig. 15 we give graphs of $\tilde{\phi}$ along the lines $b - b(\tilde{x} \leqq 0, \tilde{y} = 0)$ and $c - c(\tilde{x} = 0, \tilde{y} \leqq 0)$ for $\eta = 0, .05$, and .1. In Fig. 16 we give a vector plot of the field around the plate for $\eta = .1$.

Finally, we have numerically evaluated the integral (27) in order to

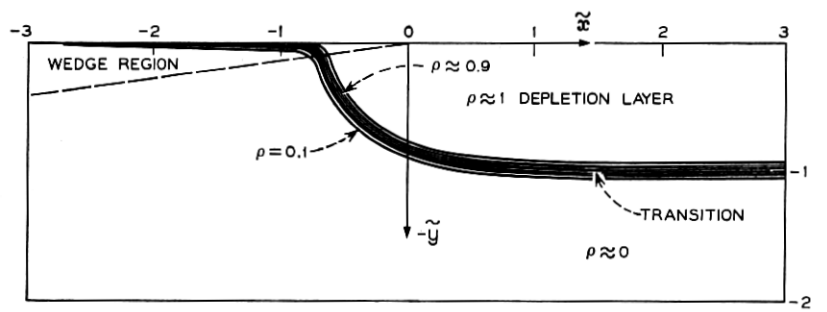

Fig. 13—Constant charge density curves for the case $\eta = .1$, $\phi_0 = -500$, and $\tilde{a} = 3$.

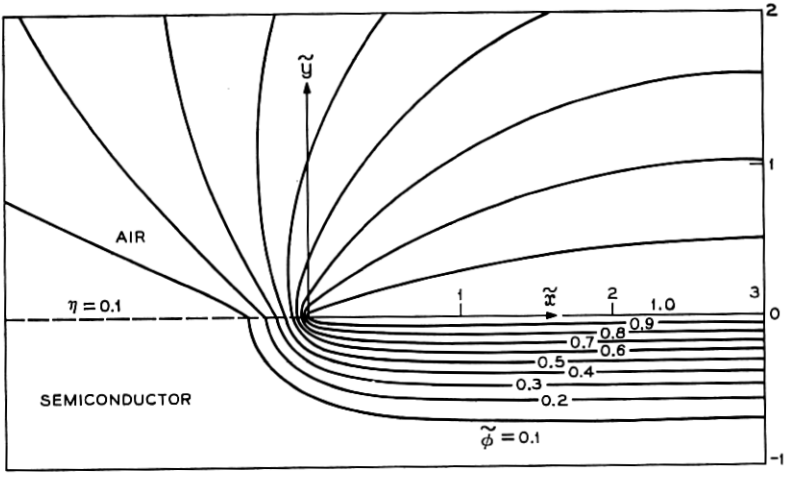

Fig. 14—Equipotential curves for the case $\eta = .1$, $\phi_0 = -500$, and $\tilde{a} = 3$.

calculate the capacitance for $\eta \neq 0$. This was done for $\phi_0 = -500$, $\tilde{a} = 3$, for $\eta = 0$, .05, and .1 with $\Delta\tilde{x} = \Delta\tilde{y} = .05$, and for $\eta = 0$, .05, .1, .15 and .2 with $\Delta\tilde{x} = \Delta\tilde{y} = .1$. For this range of values of η, it was found that (27) and the expressions (31) and (37) for the capacitance remain valid if $D_0 = .354$ is replaced by

$$D(\eta) = .354 + .43\ \eta. \tag{39}$$

We believe the number .43 in equation (39) is correct to about 10 percent.

If we had approximated the depletion layer by a rectangle with sides $2a^*$ and R^* completed at each end with a quarter circle of radius R^*, we would have obtained $D(\eta) \equiv \pi/4$. With this value of $D(\eta)$, equation (37) yields the approximation of Goodman[8] and of Sze and Gibbons.[9] By a completely different technique Copeland[10] has independently obtained the values $D(.078) = .375$ and $D(.0625) = .365$ which agree rather well with our results.

IV. DETAILS OF THE NUMERICAL METHODS

In this section we discuss some of the details of the various finite difference schemes used in solving numerically the boundary value problems P1 and P2. In each of the three cases studied, $\eta = 0$ and $|\phi_0| \ll 1$, and $\eta \neq 0$, $|\phi_0| \gg 1$, the basic nonlinear partial differential equation (6) or (20) is replaced by a system of finite difference equations,

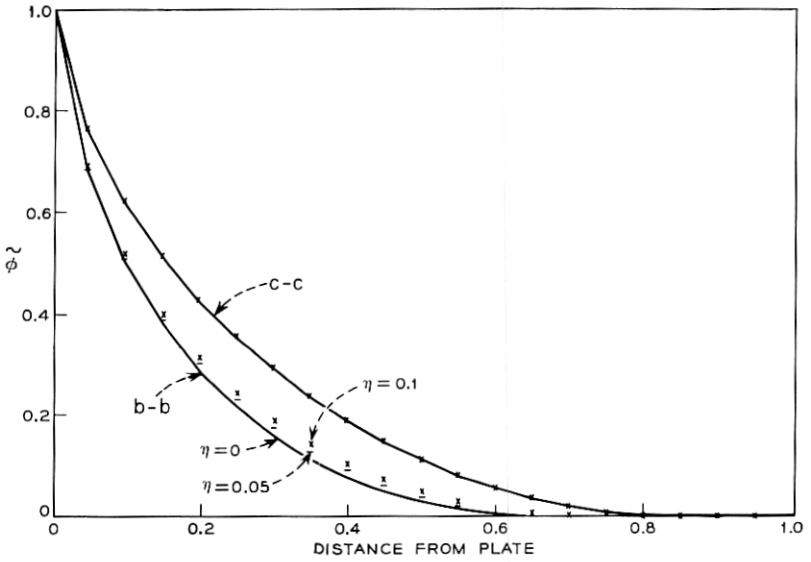

Fig. 15—Graphs of $\tilde{\phi}$ along the lines $b - b$ ($\tilde{x} \leqq 0$, $\tilde{y} = 0$) and $c - c$ ($\tilde{x} = 0$, $\tilde{y} \leqq 0$) for the case $\phi_0 = -500$ and $\tilde{a} = 3$ for $\eta = 0$, .05, and .1.

but the boundary conditions, or the method of solving the finite difference equations differ from case to case.

In each case the infinite plane is replaced by a finite rectangle, as shown in Fig. 17, where advantage is taken of the symmetry of the problem around $x = a$. The rectangle is subdivided into a square mesh with mesh spacing h, so the rectangle has length Mh and depth Nh. In the small potential case, we define

$$\phi_{i,j} = \phi(a - (i - 1)h, -(j - 1)h, \tag{40a}$$

while in the large potential case

$$\phi_{i,j} = \tilde{\phi}(\tilde{a} - (i - 1)h, -(j - 1)h), \tag{40b}$$

where $(1 \leqq i \leqq M + 1, 1 \leqq j \leqq N + 1)$. In either case, at each interior mesh point, $\nabla^2\phi_{i,j}$ is approximated by the five point formula[6]

$$\nabla_h^2\phi_{i,j} = (\phi_{i+1,j} + \phi_{i-1,j} + \phi_{i,j+1} + \phi_{i,j-1} - 4\phi_{i,j})/h^2 . \tag{41}$$

At the boundary points ($i = 1$, $2 \leqq j \leqq N$) we make use of the basic symmetry to write

$$\nabla_h^2\phi_{1,j} = (2\phi_{2,j} + \phi_{1,j+1} + \phi_{1,j-1} - 4\phi_{1,j})/h^2 , \tag{42}$$

and similarly in the case $\eta = 0$ we write

$$\nabla_h^2 \phi_{i,1} = (\phi_{i+1,1} + \phi_{i-1,1} + 2\phi_{i,2} - 4\phi_{i,1})/h^2 \tag{43}$$

for $(M_1 + 1 < i \leqq M)$, where $M_1 h = a$ for $|\phi_0| \ll 1$ and $M_1 h = \tilde{a}$ for $|\phi_0| \gg 1$.

When $\eta = 0$, $|\phi_0| \ll 1$, equation (6) is replaced by the difference equations

$$\nabla_h^2 \phi_{i,j} = \exp(-|\phi_{ij}|) - 1 \tag{44}$$

for $(1 \leqq i \leqq M,\ 2 \leqq j \leqq N)$ and $(M_1 + 1 < i \leqq M,\ j = 1)$. Since $\phi \leqq 0$ everywhere, the replacement of $\exp \phi$ by $\exp -|\phi|$ changes nothing analytically, but numerically it eliminates certain instabilities in some iteration schemes. Equation (43) must be supplemented by further equations obtained from the boundary conditions. The condition $\phi = \phi_0$ on the strip yields

$$\phi_{i,1} = \phi_0, \qquad (1 \leqq i \leqq M_1 + 1). \tag{45}$$

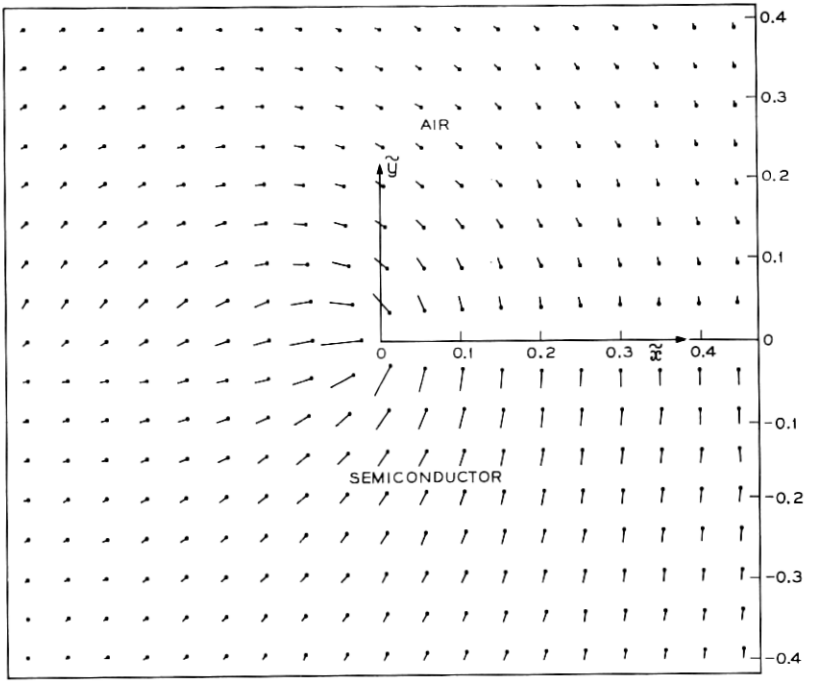

Fig. 16—A vector plot of the field around the edge of the plate for the case $\eta = .1$, $\phi_0 = -500$, and $\tilde{a} = 3$. Each line segment has the direction of the field and the length of the segment is proportional to the magnitude of the field.

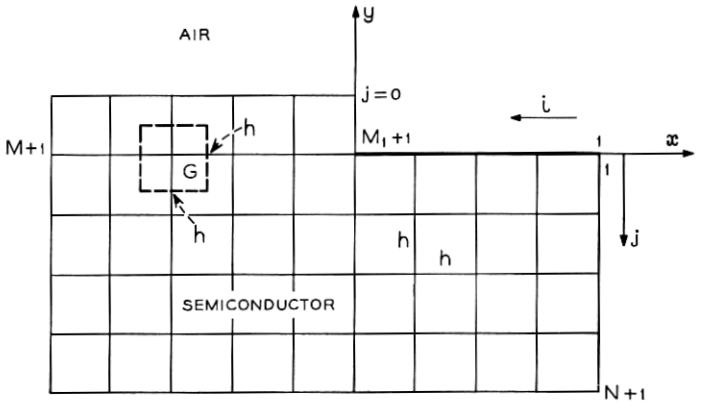

Fig. 17—A schematic drawing of the square grid used in the numerical calculations.

On the remaining boundaries condition (11) is approximated by requiring the vanishing of the normal derivatives, which decay faster than the potential itself. This yields the finite difference equations

$$\phi_{M+1,j} = \phi_{M,j} , \qquad (1 \leqq j \leqq N), \tag{46}$$

$$\phi_{i,N+1} = \phi_{i,N} , \qquad (1 \leqq i \leqq M). \tag{47}$$

Equations (44), (45), (46) and (47) form a system of $MN + M + N$ equations for the values of $\phi_{i,j}$ at $MN + M + N$ mesh points ($\phi_{M+1,N+1}$ does not appear in these equations).

This set of transcendental equations has a unique solution[11] which was determined numerically by a point successive over-relaxation iterative method.[12,13] Briefly described, the method is as follows: an initial guess, $\phi_{i,j}^{(0)}$, is made for $\phi_{i,j}$. At each interior point subsequent iterations $\phi_{i,j}^{(n)}$ are determined by the equations

$$\bar{\phi}_{i,j}^{(n+1)} = \tfrac{1}{4}\{\phi_{i+1,j}^{(n)} + \phi_{i-1,j}^{(n+1)} + \phi_{i,j+1}^{(n)} + \phi_{i,j-1}^{(n+1)} - h^2 \exp(-|\phi_{i,j}^{(n)}|) + h^2\}, \tag{48}$$

$$\phi_{i,j}^{(n+1)} = \omega\bar{\phi}_{i,j}^{(n+1)} + (1 - \omega)\phi_{i,j}^{(n)} . \tag{49}$$

The over-relaxation parameter ω is given by [13]

$$\omega = 1 + \sigma^2/[1 + (1 - \sigma^2)^{\frac{1}{2}}]^2 \tag{50a}$$

$$\sigma = \tfrac{1}{2}\{\cos(\pi/N) + \cos(\pi/M)\}. \tag{50b}$$

This value of ω is optimal for the Dirichlet problem for Laplace's

equation. Equation (48) must be modified in an obvious way at the boundary points where (44) is satisfied, and the $\phi_{i,j}$ at the remaining boundary points must be eliminated with the aid of equations (45) through (47). The iterations are repeated until either

$$\delta_\infty = \{\max_{i,j} | \phi_{i,j}^{(n+1)} - \varphi_{i,j}^{(n)} |\}/| \phi_0 | \tag{51a}$$

or

$$\delta_2 = \{\sum_i \sum_j | \phi_{i,j}^{(n+1)} - \phi_{i,j}^{(n)} |^2\}^{\frac{1}{2}}/\{| \phi_0 | (MN + M + N)^{\frac{1}{2}}\} \tag{51b}$$

is suitably small. It is important to note that the nonlinear term, $\exp(\phi_{i,j})$, appears on the right hand side of equation (48). For this reason the method is referred to as an explicit scheme. Typically in the small potential case we chose $M_1 = 40$, $M = 100$, $N = 92$, $h = .1$, and $\phi_{i,j}^{(0)} = 0$, and after 50 iterations we obtained $\delta_\infty < 10^{-3}$ and $\delta_2 < 10^{-4}$.

The iteration scheme just outlined is only conditionally stable, and it can be shown that an approximate condition for its convergence when applied to a system of equations of the form

$$\nabla_h^2 \phi_{i,j} = f(\phi_{i,j}) \tag{52}$$

is

$$\omega\left(1 + \frac{h^2 C}{4}\right) < 2, \tag{53a}$$

where

$$C = \max f'(\phi). \tag{53b}$$

When $| \phi_0 | \ll 1$, condition (53a) does not impose a severe restriction, since the region over which the solution varies significantly is small. Then h, M and N can be chosen so that M and N are not too large and at the same time h and ω satisfy equation (52) for economically acceptable ω. When $| \phi_0 | \gg 1$, however, the depletion layer is so large that M and N must be chosen excessively large in order for (52) to be satisfied.

In order to avoid this difficulty, we have employed an implicit scheme instead of an explicit one. For convenience we first introduce rescaled (tilde) coordinates in (19). For $\eta = 0$, the resulting finite difference equations are just those given in equations (41) through (47) except that (44) is replaced by

$$\nabla_h^2 \phi_{i,j} = 2\{1 - \exp(-| \phi_0 \phi_{ij} |)\}. \tag{54}$$

The explicit iteration scheme defined by equations (48) and (49) is replaced by the following implicit scheme. The quantity $\bar{\phi}_{i,j}^{(n+1)}$ is now the root of the transcendental equation

$$\bar{\phi}_{i,j}^{(n+1)} - \frac{h^2}{2} \exp\{-|\phi_0 \bar{\phi}_{i,j}^{(n+1)}|\} = \tfrac{1}{4}\{\phi_{i+1,j}^{(n)} + \phi_{i-1,j}^{(n+1)} + \phi_{i,j+1}^{(n)} + \phi_{i,j-1}^{(n+1)} - 2h^2\}. \quad (55)$$

The solution of this equation, which can be found by the Newton–Raphson method, is then substituted into equation (49) to obtain $\phi_{i,j}^{(n+1)}$. Equation (55) must be modified in an obvious way at the boundary points where (43) is satisfied, and the $\phi_{i,j}$ at the remaining boundary points are eliminated as before. When $0 < \omega < 2$, the iteration scheme just defined can be shown to be unconditionally stable,[12] that is, it converges for any mesh size h and any $\phi_{i,j}^{(0)}$. However, in practice we found $\omega \sim 1.5$ to provide the most rapid convergence. The rapidity of convergence is not very sensitive to small changes in ω around $\omega = 1.5$. Typically in the large potential case for $\eta = 0$ we chose $M_1 = 60$, $M = 100$, $N = 40$, and $h = .05$, and after $\sim$80 iterations we obtained $\delta_\infty < 10^{-4}$ and $\delta_2 < 1.6 \times 10^{-5}$.

When $\eta \neq 0$, this iteration scheme must be modified to take into account the coupling of the potential in the semiconductor to the potential in the air. If we attempt to solve directly for the potential in both the air and in the semiconductor by the method of finite differences, we encounter difficulties. The potential in the air decays very slowly at infinity, so that if we use a reasonable number of mesh points, boundary conditions such as (46) and (47) introduce fairly large errors into the calculation. In order to circumvent this problem without using an inordinately large number of mesh points we proceed as follows. We replace boundary condition (8b) by the equivalent condition that[4]

$$-\int_{\partial G} \epsilon \frac{\partial \phi^*}{\partial n^*}\, dl^* = \int_G \int \rho^*\, dx^*\, dy^*, \quad (56)$$

where G is a small square shown in Fig. 17, of side h centered at the boundary point ($M_1 + 1 < i < M$, $j = 1$). The integral on the left of equation (56) is a line integral around the boundary of G, and $\partial/\partial n^*$ denotes the normal derivative. The finite difference approximation to (56) yields the equation in tilde coordinates

$$\phi_{i,2} + \eta\phi_{i,0} + \frac{(1+\eta)}{2}(\phi_{i+1,1} + \phi_{i-1,1}) - 2(1+\eta)\phi_{i,1} = h^2\{1 - \exp(-|\phi_0\phi_{i,1}|)\}, \quad (57)$$

where $\phi_{i,0}$ is the potential at the mesh point in the air ($y = h$). Equation (57) now replaces (43) at the air-semiconductor interface points, and yields the iteration equations

$$\bar{\phi}_{i,1}^{(n+1)} - \frac{h^2 \exp\left(-|\phi_0 \bar{\phi}_{i,1}^{(n+1)}|\right)}{2(1+\eta)} = \tfrac{1}{4}\{\phi_{i-1,1}^{(n+1)} + \phi_{i+1,1}^{(n)}\}$$

$$+ \frac{1}{2(1+\eta)}\{\eta\phi_{i,0}^{(n)} + \phi_{i,2}^{(n)} - h^2\}, \qquad (M_1 + 1 < i < M). \tag{58}$$

Once the $(n+1)$ iterates $\phi_{i,j}^{(n+1)}$ have been determined for all points within and on the boundary of the semiconductor, the $\phi_{i,0}^{(n+1)}$, $(M_1 + 1 < i \leqq M)$, are calculated from the finite difference version of Green's formula (38) using the values $\phi_{i,1}^{(n+1)}$ already known. We did not prove that this modified iteration scheme converges, but it works well in practice. In this case also, the empirically determined value $\omega = 1.5$ seems optimal.

Finally, we make several brief comments about the difference between the true solutions of P1 or P2 and the numerical solutions, that is, the truncation errors. It is well known[13] that when the true solution is smooth enough (specifically when the fourth derivatives are bounded) the truncation error is $O(h^2)$. However, in our problem, near the plate's edge $x = y = 0$, even the first derivative is not bounded, and the above estimate fails. Wasow[14] considered a problem similar to ours with smooth boundaries and piecewise analytic boundary values and found that the truncation error vanished when $h \to 0$.

It can be shown[15] that near the corner $x = y = 0$, the singularity in the field for arbitrary η is

$$\nabla\phi = O(r^{-\frac{1}{2}}) \tag{59}$$

for both the small and large potential cases (in the appropriate coordinates) where r is the distance from the corner. Bramble, and others,[16] investigated the truncation (or discretization) error of such problems, and if we combine equation (59) with their Theorem 3.1, we find that near the corner the truncation error is

$$|\phi_{i,j} - \phi_{\text{exact}}(x, y)| = O(h^{\frac{1}{2}}), \tag{60}$$

and it vanishes as $h \to 0$.

The truncation error is not uniform, and because of the slow convergence near the corner, it is worthwhile to refine the mesh size in a small region around it (as was described in Section II). This was done for the small potential case for $\eta = 0$ and $\phi_0 = -.01$, for a refined mesh size of $h = .0125$ and in Fig. 18 we compare the analytic solution

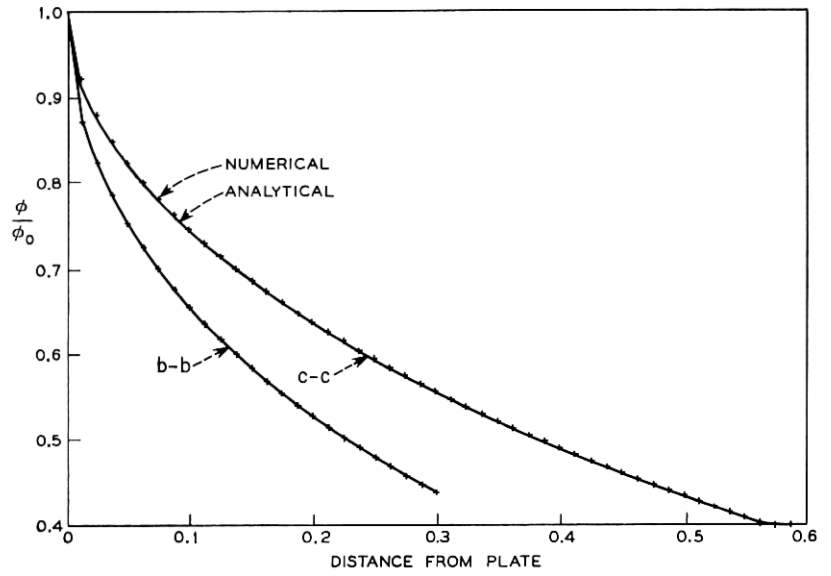

Fig. 18—A comparison of the analytical solution of the linearized problem (continuous line) with the numerical solution of the nonlinear problem P2 (crosses) for the case $\eta = 0, \phi_0 = .01$ and for a mesh size near the plate edge of $\Delta x = \Delta y = .0125$.

(continuous line) with the numerical one (crosses) along the lines $b - b$ and $c - c$.

All the calculations described in this paper were performed on a GE 635 digital computer. The graphical output was obtained with the aid of a routine for calculating level curves written by G. S. Deem, L. K. Russell, and N. J. Zabusky.[17]

V. ACKNOWLEDGMENTS

The authors are indebted to H. K. Gummel, J. A. Lewis, E. G. Nicolian, R. J. Strain and S. Sze for many helpful conversations during the work on this problem. They also wish to acknowledge the expert assistance of Miss C. G. Miller in efficiently translating into computer programs the many numerical schemes proposed.

REFERENCES

1. Lewis, J. A., McKenna, J., and Wasserstrom, E., "The Field of Negative Point, Line or Plane Charges in an n-Type Semiconductor," unpublished work.
2. Sze, S., *Physics of Semiconductor Devices*, New York: John Wiley and Sons, Inc., 1969, pp. 368, 370.

3. Landau, L. D., and Lifshitz, E. M., *Statistical Physics*, London: Pergamon Press, 1968, p. 231.
4. Panofsky, W. K. H., and Phillips, M., *Classical Electricity and Magnetism*, Cambridge, Mass.: Addison-Wesley Publishing Co., 1955, pp. 26, 27.
5. Lewis, J. A., "The Flat Plate Problem for a Semiconductor," to be published in the September 1970 issue of the B.S.T.J.
6. Abramowitz, M., and Stegun, I. A., *Handbook of Mathematical Functions*, Washington: National Bureau of Standards, 1964, pp. 297, 885.
7. Titchmarsh, E. C., *Theory of Fourier Integrals*, Oxford: Oxford University Press, 1948, p. 125.
8. Goodman, A. M., "Metal-Semiconductor Barrier Height Measurement by the Differential Capacitance Method-Ore Carrier System," *J. Appl. Phys.*, *34*, No. 2(February 1963), p. 329.
9. Sze, S. M., and Gibbons, G., "Effect of Junction Curvature on Breakdown Voltage in Semiconductors," Solid-State Electronics, *9*, No. 9 (September 1966), p. 831.
10. Copeland, J. A., "Diode Edge Effect on Doping-Profile Measurement," IEEE Trans. Electron Devices, *ED-17*, No. 5 (May 1970).
11. Bers, L., "On Mildly Nonlear Partial Difference Equations of Elliptic Type,'' J. Research Natl. Bur. Standards, *51*, No. 11 (November 1953), p. 229.
12. Ortega, J. M., and Rockoff, M. L., "Nonlinear Difference Equations and Gauss-Seidel Type Iterative Methods," J. SIAM Numer. Anal., *3*, No. 9 (September 1966), p. 497.
13. Varga, R. S., *Matrix Iterative Analysis*, Englewood Cliffs, N. J.: Prentice-Hall, 1962, pp. 59, 165, 203.
14. Wasow, W. R., "The Accuracy of Difference Approximations to Plane Dirichlet Problems with Piecewise Analytic Boundary Values," Quart. Appl. Math., *15*, No. 4 (April 1957), p. 53
15. Lewis, J. A., and Wasserstrom, E., "The Field Singularity at the Edge of an Electrode on a Semiconductor Surface," to be published in the July-August 1970 issue of the B.S.T.J.
16. Bramble, J. H., Hubbard, B. E., and Zlamal, M., "Discrete Analogues of the Dirichlet Problem with Isolated Singularities," SIAM J. Numer. Analy., *5*, No. 3 (March 1968), p. 1.
17. Deem, G. S., Russell, L. K., and Zabusky, N. J., unpublished work.